Woodhead Publishing Series in Energy

Molten Salt Reactors and Thorium Energy

Second Edition

Edited by

THOMAS JAMES DOLAN

IMRE PÁZSIT

ANDREI RYKHLEVSKII

RITSUO YOSHIOKA

ELSEVIER

WP WOODHEAD PUBLISHING

An imprint of Elsevier

Woodhead Publishing is an imprint of Elsevier
50 Hampshire Street, 5th Floor, Cambridge, MA 02139, United States
125 London Wall, London EC2Y 5AS, United Kingdom

Notices

Knowledge and best practice in this field are constantly changing. As new research and experience broaden our understanding, changes in research methods, professional practices, or medical treatment may become necessary.

Practitioners and researchers must always rely on their own experience and knowledge in evaluating and using any information, methods, compounds, or experiments described herein. In using such information or methods they should be mindful of their own safety and the safety of others, including parties for whom they have a professional responsibility.

To the fullest extent of the law, neither the Publisher nor the authors, contributors, or editors, assume any liability for any injury and/or damage to persons or property as a matter of products liability, negligence or otherwise, or from any use or operation of any methods, products, instructions, or ideas contained in the material herein.

ISBN: 978-0-323-99355-5 (print)
ISBN: 978-0-323-99356-2 (online)

For information on all Woodhead Publishing publications
visit our website at https://www.elsevier.com/books-and-journals

Publisher: Megan Ball
Editorial Project Manager: Joshua Mearns
Production Project Manager: Fizza Fathima
Cover Designer: Greg Harris

Typeset by MPS Limited, Chennai, India

Contents

List of contributors *xxi*
Preface to the second edition *xxv*
Preface to the first edition *xxvii*

Part 1 Applications

Editor: THOMAS JAMES DOLAN

1. Introduction **3**
Thomas James Dolan
1.1 Need for molten salt reactor 3
1.2 Molten salt reactor origin and research curtailment 4
1.3 Molten salt reactor activities 5
1.4 Fissile fuels 6
1.5 Thorium fuel advantages 7
1.6 Liquid fuel molten salt reactor 8
1.7 Advantages of liquid fuel molten salt reactor 10
1.7.1 Safety advantages 10
1.7.2 Economic advantages 11
1.7.3 Environmental advantages 12
1.7.4 Nonproliferation advantages 13
1.8 Molten salt reactor development issues 13
1.9 Tritium issues 15
References 16

2. Electricity production **19**
Lindsay Dempsey and Charles Forsberg
2.1 Electricity production 20
2.2 Energy storage for electricity production 21
2.3 Heat engines 26
2.4 Rankine cycle (steam turbines) 29
2.5 Helium Brayton cycles 31
2.6 Supercritical CO_2 Brayton cycles 33
2.7 Metal vapor binary cycles 34
2.7.1 Mercury/steam binary cycle 34
2.7.2 Potassium/steam binary cycle 35
2.8 Nuclear air Brayton power cycles 35
2.9 Summary 43
References 44

3. Other applications **47**

Stephen Boyd and Christopher Taylor

3.1 Introduction 48
3.2 Remote power sources 48
3.2.1 Historical context 48
3.2.2 Nuclear powered marine propulsion 48
3.2.3 Radioisotope thermoelectric generators and betavoltaic cells as remote power sources: extracting electrical work from molten salt properties waste 49
3.2.4 Space-based nuclear reactors as remote power sources 51
3.2.5 Materials considerations for space-based molten salt properties 53
3.2.6 Fueling the molten salt properties on Mars and its employment as elemental production platform 56
3.3 Heat exchangers 60
3.4 High-temperature commercial applications 61
3.4.1 Ammonia production 61
3.4.2 Hydrogen production 64
3.4.3 Catalytic cracking 67
3.5 Actinide burning 69
3.5.1 Historical context 69
3.5.2 Fluoride preprocessing and spent nuclear fuel fission 70
3.6 Medical isotopes 70
3.7 Desalination 71
3.7.1 Desalination plant types 72
3.7.2 Global reliance on desalinated water and the nuclear role 72
3.7.3 Comparison of nuclear versus renewables for desalination 74
3.7.4 Nuclear versus renewables financial perspective 77
3.8 Optical applications 78
3.9 Summary and conclusions 78
Acknowledgment 80
References 80

Part 2 Technical issues

Editor: IMRE PÁZSIT

4. Molten salt reactor physics: characterization, neutronic performance, multiphysics coupling, and reduced-order modeling **87**

Jiri Krepel and Jean C. Ragusa

4.1 Molten salt reactor characterization and neutronic performance 87

4.1.1 Definition and taxonomy 88
4.1.2 Neutronic characterization of considered nuclides 89
4.1.3 Reactor physics characterization 98
4.1.4 Neutronic performance parameters 106
4.1.5 Fuel cycle types, core sizes, and performance 121
4.1.6 Safety relevant features 134
4.2 Molten salt reactor multiphysics coupling and reduced-order modeling 144
4.2.1 Various aspects of multiphysics coupling in molten salt reactors 146
4.2.2 Governing laws 151
4.2.3 Reduced-order model 162
References 191

5. Kinetics, dynamics, and neutron noise in stationary molten salt reactors 199

Imre Pázsit and Victor Dykin

5.1 Introduction 200
5.2 The molten salt reactor model 202
5.3 The static equations 204
5.3.1 The adjoint property 204
5.3.2 Interpretation of the equation and some limiting cases 206
5.3.3 The case of no recirculation 208
5.3.4 The case of infinite fuel velocity 208
5.3.5 The full solution 210
5.3.6 Alternative solution of the molten salt reactor equations 212
5.3.7 Quantitative results 213
5.4 Space-time-dependent transient during startup 215
5.4.1 The space-time-dependent equations for the transient 216
5.4.2 Solution for $u \to \infty$ 221
5.5 Dynamic equations in the frequency domain: neutron noise 231
5.5.1 The Green's function 234
5.5.2 Solution for $u = \infty$ 235
5.5.3 Quantitative analysis: comparison with traditional systems 236
5.5.4 Results with finite velocity 239
5.6 The point kinetic approximation and the point kinetic component 240
5.6.1 Introduction and background 241
5.6.2 Derivation of the linearized point-kinetic equations 243
5.6.3 Point kinetic equation with static fluxes 249
5.6.4 Derivation of the point kinetic component from the full solution 251

5.7 The neutron noise in a molten salt reactor, induced by propagating perturbations 254
5.8 Conclusions 258
Acknowledgment 259
References 259

6. Thermal hydraulic analysis of liquid-fueled molten salt reactors 263

Antonio Cammi, Valentino Di Marcello, Alessandro Pini and Lelio Luzzi

6.1 Introduction 263
6.2 Preliminary approach to thermohydraulics of internally heated molten salts 265
6.2.1 Analytic framework for validation purposes 265
6.2.2 Laminar flow 267
6.2.3 Turbulent flow 267
6.3 Heat transfer and pressure losses 269
6.3.1 Laminar flow 272
6.3.2 Turbulent flow 273
6.4 Effects of internal heat generation on natural circulation stability 276
6.5 Conclusions 283
Acknowledgments 284
Abbreviations 284
References 284

7. Materials 289

Ritsuo Yoshioka, Motoyasu Kinoshita, Ian Scott and Christopher Taylor

7.1 Molten salt 289
7.1.1 Fluoride salt, mostly FLiBe 289
7.1.2 Other molten fluorides 295
7.1.3 Chloride salt 295
7.2 Solid fuels with molten salt coolants 301
7.3 Thorium fuel cycle 301
7.4 Moderators 302
7.4.1 Graphite 303
7.4.2 Beryllium 304
7.4.3 Lithium 306
7.5 Structural materials 308
7.5.1 Requirements for good structural materials 308
7.5.2 Development of corrosion-resistant alloys 309
7.5.3 Reduction of the corrosive potential of molten salts 310

7.5.4 Hastelloy N and other Nickel-based superalloys 312
7.6 Corrosion of materials in molten salts 317
7.6.1 Introduction 317
7.6.2 Molten salts, alloys and materials, and current topics of research 318
7.6.3 Methods for evaluating materials performance in molten salts 319
7.6.4 Materials performance in molten salts 322
7.6.5 Heat exchangers and materials embrittlement challenges 325
7.7 Conclusions 331
References 332

8. Physical—chemical properties of molten salts and chemical technology of MSR fuel cycle 335

Stephen Boyd and Jan Uhlíř

8.1 Introduction 336
8.2 Fundamental physical—chemical properties of molten salts 336
8.2.1 What makes for a good salt? 336
8.2.2 Molten salts as working fluids in thermochemical processes 337
8.2.3 Chemistry, bonding, and electronic structure of molten salts 338
8.2.4 Phase transformations in molten salts 340
8.2.5 Crystallographic relations between the solid phase and persistent short-range order in molten salts 342
8.2.6 Soft-sphere equations of state for the molten phase: the Helmholtz equation and proposed modifications resulting from molten salt chemistry 347
8.2.7 Summary of physicochemical properties of molten salts and theoretical considerations 356
8.3 Chemical technology of molten salt reactor fuel cycle 357
8.3.1 Processing of fresh liquid fuel for molten salt reactor 358
8.3.2 Reprocessing technology of molten salt reactor fuel 360
8.3.3 Gas extraction process 362
8.3.4 Fused salt volatilization 365
8.3.5 Molten salt/Liquid metal extraction 369
8.3.6 Electrochemical separation processes 371
8.3.7 Vacuum distillation 374
8.3.8 Molten salt reactor reprocessing flowsheets 374
8.3.9 Conclusions 378
8.4 Historical overview of partitioning technology with the relation to molten salt reactor 380
References 385

9. Environment, waste, and resources **391**

Ritsuo Yoshioka, Motoyasu Kinoshita, Lars Jorgensen and Magdi Ragheb

9.1 Decay heat in thorium cycle 391
9.1.1 Introduction 391
9.1.2 Unique features of molten salt reactor decay heat 392
9.1.3 Calculation method 394
9.1.4 Component of decay heat 394
9.1.5 Other influences on decay heat calculation 397
9.1.6 Verification of decay heat calculation 397
9.1.7 Final results 398
9.1.8 Summary 398
9.2 Radiotoxicity in the thorium cycle 400
9.2.1 Introduction 400
9.2.2 Calculation method 400
9.2.3 Radiotoxicity comparison between U-core and Th-core in pressurized water reactor 401
9.2.4 Effect of online reprocessing for molten salt reactor 404
9.2.5 Radiotoxicity for pressurized water reactor mixed oxide fuel 407
9.2.6 Summary 408
9.3 Nuclear waste from ThorCon type reactors 409
9.4 Resource utilization 410
9.4.1 Thorium 410
9.4.2 Helium resource 420
9.5 Summary 423
References 423

10. Proliferation resistance and physical protection of molten salt reactor **425**

Anna Erickson and Ritsuo Yoshioka

10.1 Introduction 426
10.2 Discussion of methodologies and associated metrics and barriers 427
10.2.1 Metrics or barrier 428
10.2.2 Methodology 429
10.2.3 Nuclear facility 429
10.2.4 Nuclear material accountancy 430
10.3 Proliferation resistance of molten salt reactor 431
10.3.1 Fuel type 434
10.3.2 Coolant type 437
10.3.3 Neutron spectrum 437
10.3.4 Fuel salt type 437

10.3.5 Fuel feeding after startup 437
10.3.6 Reprocessing type 438
10.3.7 Fissile and fertile materials 444
10.3.8 Blanket loop 450
10.3.9 Addition of minor actinides 450
10.3.10 Purpose 450
10.3.11 Core structure (loop-type or tank-type) 450
10.4 Physical protection of molten salt reactor 451
10.4.1 Introduction 451
10.4.2 Design basis threat of LWR 452
10.4.3 Design basis threat of molten salt reactor 457
10.5 Conclusion 458
Acknowledgment 459
References 459

Part 3 Reactor types

Editor: RITSUO YOSHIOKA

11. Liquid fuel, thermal neutron spectrum reactors 465

Ritsuo Yoshioka and Motoyasu Kinoshita

11.1 Development of molten-salt reactor at ORNL 466
11.1.1 Liquid fuel reactor, from water to molten salt 466
11.1.2 Selection of thermal neutron spectrum 477
11.1.3 Molten salt fast-spectrum reactor 479
11.1.4 Two-fluid molten-salt reactor 482
11.1.5 Molten salt breeder reactor (MSBR), large-sized single-fluid MSBR 487
11.1.6 Denatured molten-salt reactor 493
11.1.7 Termination of molten-salt reactor development at ORNL 496
11.1.8 Summary 496
11.2 Current molten-salt reactor designs after ORNL (FUJI) 497
11.2.1 Introduction 498
11.2.2 Concept of FUJI-U3 (using ^{233}U as fissile) 499
11.2.3 Design conditions 501
11.2.4 Calculation procedure for criticality 503
11.2.5 Criticality property and main results 505
11.2.6 Computational procedure for burnup characteristics 511
11.2.7 Chemical processing of fuel salt 512
11.2.8 Power control options for FUJI 512

11.2.9 Burnup behavior of reactor characteristics 513
11.2.10 Material balance of actinides 515
11.2.11 Fission products 515
11.2.12 Fuel requirement and actinides for a 1 GWe plant 516
11.2.13 FUJI-Pu (using Pu as initial fissile) 517
11.2.14 Transmutation of minor actinides by molten-salt reactor-FUJI 518
11.2.15 super-FUJI (large sized plant) 519
11.2.16 mini-FUJI (pilot plant) 520
11.2.17 Summary of FUJI Design Results 520
11.3 Safety concept of the molten-salt reactor 522
11.3.1 Introduction 522
11.3.2 Safety concept of molten-salt reactor 523
11.3.3 Safety analysis of molten-salt reactor 526
11.3.4 Molten-salt reactor safety against Fukushima-type accident 528
11.3.5 Summary 528
11.4 Safety criteria of the molten-salt reactor 529
11.4.1 Introduction 529
11.4.2 Definition of "accident" 529
11.4.3 Safety criteria for molten-salt reactor 530
11.4.4 Summary 534
11.5 Molten-salt reactor accident analysis 534
11.5.1 Introduction 534
11.5.2 Classification of accidents 534
11.5.3 Accident to be considered 535
11.5.4 Summary 551
11.6 Regulatory guide for molten-salt reactor safety design 552
11.6.1 Overall requirements 553
11.6.2 Protection by multiple fission product barriers 555
11.6.3 Protection and reactivity control systems 558
11.6.4 Fluid systems 560
11.6.5 Reactor containment 563
11.6.6 Fuel and radioactivity control 566
11.6.7 Salt systems and control 567
11.6.8 Other design requirements 568
11.6.9 Additional design basis accidents 570
11.6.10 Several definitions 571
11.6.11 Conclusion 571

11.7 Regulatory guide for molten-salt reactor safety assessment 572
11.7.1 Introduction 572
11.7.2 Safety design assessment 573
11.7.3 Commentary on molten-salt reactor safety assessment guide 577
11.7.4 Appendix to molten-salt reactor safety assessment guide 584
11.8 Transient and safety analysis code DYMOS 585
11.9 Daily load following operation 587
11.10 Micro-sized molten-salt reactor (miniFUJI II) 588
References 589

12. Fast-spectrum, liquid-fueled reactors 595

A.A. Lizin, S.V. Tomilin, Leonid I. Ponomarev, Yu S. Fedorov and Yasuo Hirose

12.1 Carrier salt for the fast molten-salt reactor 596
12.1.1 Introduction 596
12.1.2 Physical properties of the fluoride carrier salts 596
12.1.3 The solubility of the actinide and lanthanide fluorides in the fluoride molten salts 598
12.1.4 The other essential fluoride molten-salt properties 608
12.1.5 Conclusion 611
12.2 U—Pu fast molten-salt reactor based on FLiNaK 612
12.2.1 Introduction 612
12.2.2 Carrier salt for U—Pu fast molten-salt reactor 614
12.2.3 Neutron physics of U—Pu fast molten-salt reactor 614
12.2.4 U-Pu fast molten-salt reactor nuclear fuel cycle 619
12.2.5 Conclusion 625
12.3 Feasibility of the U—Pu fast-spectrum molten-salt reactors using (Li, Na, K)F—UF_4—$TRUF_3$ fuel salts 625
12.3.1 Introduction 625
12.3.2 Preliminary survey and study 626
12.3.3 U—Pu fast-spectrum molten-salt reactors 644
12.3.4 Conclusions 654
12.4 Acknowledgments 654
12.5 Adsorption from the LiF—NaF—KF melt 654
12.5.1 Introduction 654
12.5.2 Research conditions 655
12.5.3 Adsorption of NdF_3 and ThF_4 from FLiNaK 656
12.5.4 Conclusion 659
References 660

13. Solid fuel, salt-cooled reactors **667**

Raluca Scarlat and Charalampos Andreades

13.1 Introduction: definition of the fluoride-salt-cooled high-temperature reactor concept 668
13.2 FHR designs: pool versus loop, fuel element shape, and power 671
13.2.1 PB-FHR—UC Berkeley 673
13.2.2 SmAHTR—ORNL 675
13.2.3 AHTR—ORNL 676
13.2.4 FHTR—MIT 677
13.2.5 TMSR-SF—CAS 679
13.3 Plant-level features 679
13.3.1 Less developed designs, and longer-term features 680
13.3.2 Inherent safety features and passive safety systems 681
13.4 Phenomenology unique to FHRs 684
13.5 Thermal-hydraulics 684
13.5.1 University of California, Berkeley facilities 685
13.5.2 University of New Mexico facilities 688
13.5.3 Ohio state facilities 690
13.5.4 Oak Ridge National Laboratory 692
13.5.5 Shanghai Institute of Applied Physics 692
13.5.6 Pebble dynamics and fuel handling 694
13.6 Chemistry and corrosion control 695
13.7 Neutronics 696
13.8 Tritium management 697
13.8.1 Tritium sinks 700
13.8.2 Tritium mass transport in the primary coolant circuit 701
13.8.3 Tritium absorption in the fuel elements 701
13.9 Safety analysis and licensing strategy 708
13.9.1 Safety design criteria, strategies, subordinate goals 708
13.9.2 Licensing experience from liquid metal and gas-cooled reactors 709
13.9.3 Severe accidents source term 710
13.10 Summary 711
References 712
Further reading 714

14. Static liquid fuel reactors **715**

Ian Scott

14.1 Pumped versus static fuel molten salt reactor 715

14.2 Potential advantages of static-fueled reactors 717
14.2.1 Pumps and valves 717
14.2.2 Fuel salt leaks 717
14.2.3 Heat exchangers 718
14.2.4 Drain systems 718
14.2.5 Noble metal filtration system 719
14.2.6 Gas handling system 720
14.2.7 Chemistry control and refueling 720
14.2.8 Summary 721
14.3 Convective heat transfer in molten fuel salt 721
14.4 Fuel tube materials 723
14.5 Fission products and gases 728
14.6 Static molten salt-fueled reactor options 732
14.7 Thermal spectrum static molten salt reactors 734
14.8 Fuel cycle for stable salt reactors 735
14.9 Global mix of static-fueled molten salt reactors 736
References 738

15. Accelerator-driven systems **741**

Ritsuo Yoshioka, Kazuro Furukawa, Motoyasu Kinoshita, Alexey M. Degtyarev, Andrey A. Myasnikov, Laszlo Sajo-Bohus, Eduardo D. Greaves, Toshinobu Sasa and Hector Rene Vega-Carrillo

15.1 Introduction to accelerator-driven systems 742
15.2 Accelerator molten salt breeder 743
15.3 Fast subcritical molten salt reactor for minor actinide incineration 746
15.4 Main characteristics of the subcritical molten salt reactor-B 749
15.5 Low-energy linear accelerator-driven subcritical assembly 761
15.5.1 Introduction and scope 761
15.5.2 Theory 763
15.5.3 Experimental procedure 764
15.5.4 Results and discussion 766
15.6 MYRRHA, demonstration of accelerator-driven system 767
15.7 Molten salt fuel accelerator-driven system 769
15.8 Laser-driven subcritical Th-molten salt reactor 770
15.8.1 Introduction 770
15.8.2 Conceptual design of Th-molten salt reactor driven by external neutron source 772
15.8.3 Target normal sheath acceleration mechanism 774
15.8.4 Experimental results 775
15.8.5 Neutron spectra estimation by Monte Carlo method 777

15.8.6 Discussion and conclusion 782
15.9 Conclusions 783
Acknowledgments 784
References 785

16. Fusion-fission hybrids **789**

E.P. Velikhov and Ritsuo Yoshioka

16.1 Energy needs 789
16.2 Fast breeder reactors 790
16.3 Fusion-fission hybrids 790
16.4 Thorium fuel cycle 794
16.5 Nuclear energy system 795
16.6 Actinide incineration 797
16.7 Molten salt hybrid tokamak 798
References 799

Part 4 Reactor designs

Editor: ANDREI RYKHLEVSKII

17. Thorium molten salt reactor nuclear energy system **803**

Zhimin Dai

17.1 Introduction 803
17.2 Liquid-fueled thorium molten salt reactor 804
17.2.1 Design overview of liquid-fueled thorium molten salt reactor 804
17.2.2 Safety features of liquid-fueled thorium molten salt reactor 806
17.2.3 Advanced Th-U fuel cycle based on liquid-fueled thorium molten salt reactor 807
17.3 Solid-fueled thorium molten salt reactor 809
17.3.1 Design overview of solid-fueled thorium molten salt reactor 809
17.3.2 Safety features of solid-fueled thorium molten salt reactor 811
17.3.3 Multipurpose utilization of nuclear energy based on solid-fueled thorium molten salt reactor 813
17.4 Summary 814

18. Integral molten salt reactor **815**

David LeBlanc and Cyril Rodenburg

18.1 Introduction 815
18.2 Description of nuclear systems 817
18.3 Description of safety concept 819

18.4 Proliferation defenses 823
18.5 Safety and security (physical protection) 824
18.6 Description of turbine generator systems 825
18.7 Electrical and I&C systems 825
18.8 Spent fuel and waste management 826
18.9 Plant layout 827
18.10 Plant performance 827
18.11 Development status of technologies relevant to the power generation 828
18.12 Deployment status and planned schedule 829
Appendix: Summarized technical data 830
Further reading 833

19. ThorCon reactor 835

Lars Jorgensen and Robert Hargraves

19.1 Need for deployment 835
19.2 Modular power plant 836
19.3 Power conversion 839
19.4 Safety features 840
19.4.1 Passive, unavoidable shutdown and cooling 840
19.4.2 Radioactivity release resistance 841
19.5 Maintenance 841
19.6 Molten salt reactor experiment versus coal 841
19.7 Construction speed 842
19.7.1 No new technology is required 842
19.7.2 Historical examples 842
19.7.3 Shipyard quality and productivity 843
References 845

20. Severe accident modeling and safety assessment for fluid-fuel energy reactors 847

Jan L. Kloosterman

20.1 Objectives of the project 848
20.2 The concept of the molten salt fast reactor 849
20.3 Main research themes 852
20.4 The SAMOSAFER consortium 854
20.4.1 Universities 854
20.4.2 National laboratories 854
20.4.3 Industry, utilities, and TSO 856
Reference 856

21. Stable salt fast reactor **857**

Ian Scott

21.1 Design principles 857
21.2 Design outline 858
21.3 Fuel salt 860
21.4 Primary coolant salt 861
21.5 Secondary heat transfer loop and steam island 862
21.6 Fuel management and refueling 863
21.7 Neutronics and reactivity control 864
21.8 Decay heat removal 865
21.9 Waste and spent fuel management 867
21.10 Breeding potential 868
21.11 Conclusions 868
Reference 869

22. EXODYS Fast-Chloride Molten Salt Reactor **871**

Edward Pheil and Carl Perez

22.1 Introduction 872
22.2 Description of the nuclear systems 874
22.2.1 Core design 875
22.2.2 Heat transfer module 877
22.2.3 Surrounding salt tank 878
22.3 Safety systems 880
22.3.1 Emergency shutdown 880
22.3.2 Decay heat removal 881
22.3.3 Containment 882
22.3.4 Seismic resistance 883
22.4 Salt chemistry systems 884
22.4.1 Fuel salt production 884
22.4.2 Molten salt control 886
22.4.3 Fission product removal 887
22.4.4 Fission salt conditioning 889
22.5 Plant configuration and operation 890
22.5.1 Plant layout 890
22.5.2 Operation and maintenance 891
22.5.3 Decommissioning 893
22.6 Summary 893
References 895

23. Copenhagen atomics waste burner **897**

Thomas Jam Pedersen

23.1 Reactor design choices 898
23.2 Mechanical design choices 900
23.3 Recycling of used nuclear fuel 902
23.4 Molten salt reactor engineering 903
23.5 Molten salt reactor research 904
23.6 "Prime minister safety" 905
Reference 906

24. Seaborg technologies ApS—compact molten salt reactor power barge **907**

Troels Schønfeldt, Esben Klinkby, Andreas Vigand Schofield, Eirik Eide Pettersen and Federico Puente-Espel

24.1 Introduction 907
24.2 Design description 909
24.2.1 Seaborg design philosophy 909
24.2.2 Compact molten salt reactor 910
24.2.3 Compact molten salt reactor power barge 914
24.3 Plant arrangement 916
24.4 Plant economics 917
Reference 918

25. Dual-fluid reactor **919**

Armin Huke, Götz Ruprecht, Daniel Weißbach, Konrad Czerski, Stephan Gottlieb, Ahmed Hussein, Dominik Böhm and Nico Bernt

25.1 The dual-fluid technology 919
25.2 Fuel cycle: the pyroprocessing unit 923
25.3 Applications 925
25.4 Electricity production 925
25.5 Synthetic fuels 926
25.6 Hydrazine for combustion and fuel cells 926
25.7 Silane 927
25.8 Other applications 927
25.8.1 Radiotomic chemical production 927
25.8.2 Medical isotope production 927
25.8.3 Neutron source for science and industry 928
25.9 Structural materials 928
25.10 Energy return on investment 929

25.11 Variants and scaling of the dual fluid reactor 933
25.11.1 The DF300, a small modular reactor 933
25.11.2 The DF1500, a replacement for conventional LWR 933
25.11.3 The DF30G, a high-temperature heat source for large chemical process plants 935
25.12 Comparison with other reactor types 936
References 942
Further reading 943

26. Kairos power pebble bed reactor 945
Andrei Rykhlevskii

26.1 Introduction 945
26.2 Company overview 945
26.3 Technical description 946
26.4 Safety features 949
26.5 Hermes demonstration reactor 950
26.6 Summary and path forward 951
References 952

27. TerraPower fast chloride reactor 953
Jiri Krepel and Kevin J. Kramer

27.1 Introduction 953
27.2 Historical background 955
27.3 Current molten chloride fast reactor development 957
27.4 Technical description 961
27.5 Operational, safety and public acceptance features 964
27.5.1 Safeguards and nonproliferation 967
27.5.2 Economic competitiveness 967
27.6 Summary and path forward 969
References 970

28. Conclusions 973
Thomas James Dolan

28.1 Achievements 973
28.2 Reactor development 975
28.3 Societal issues 976
28.4 Conclusions 976

Appendix A: Abbreviations *977*
Index *989*

List of contributors

Charalampos Andreades
University of California, Berkeley, CA, United States

Nico Bernt
Institute for Solid-State Nuclear Physics, Berlin, Germany

Dominik Böhm
Institute for Solid-State Nuclear Physics, Berlin, Germany

Stephen Boyd
Aufbau Laboratories, LLC, Manhasset, NY, United States

Antonio Cammi
Politecnico di Milano – Energy Department – Nuclear Engineering Division – CeSNEF (Enrico Fermi Centre for Nuclear Studies), Milano, Italy

Konrad Czerski
Institute for Solid-State Nuclear Physics, Berlin, Germany; University of Szczecin, Szczecin, Poland

Zhimin Dai
Shanghai Institute of Applied Physics, Shanghai, P.R. China

Alexey M. Degtyarev
NRC "Kurchatov Institute," Moscow, Russia

Lindsay Dempsey
Generation Solutions, Calgary, AB, Canada

Valentino Di Marcello
National Institute for Nuclear Physics – Gran Sasso National Laboratory (LNGS), Assergi, Italy

Thomas James Dolan
University of Illinois at Urbana-Champaign, Urbana, IL, United States

Victor Dykin
Chalmers University of Technology, Department of Physics, Division of Subatomic, High Energy and Plasma Physics, Göteborg, Sweden

Anna Erickson
Georgia Institute of Technology, Atlanta, GA, United States

Yu S. Fedorov
Petersburg State Technological Institute (Technical University), St. Petersburg, Russia

Charles Forsberg
Massachusetts Institute of Technology, Cambridge, MA, United States

Kazuro Furukawa
High Energy Accelerator Research Organization, ITMSF, Tsukuba, Japan

Stephan Gottlieb
Institute for Solid-State Nuclear Physics, Berlin, Germany

Eduardo D. Greaves
Universidad Simon Bolivar, Caracas, Venezuela

Robert Hargraves
ThorCon US, Inc., Cheyenne, WY, United States

Yasuo Hirose
Institute of Innovative Research, Kashiwa, Japan

Armin Huke
Institute for Solid-State Nuclear Physics, Berlin, Germany

Ahmed Hussein
Institute for Solid-State Nuclear Physics, Berlin, Germany; University of Northern British Columbia, Prince George, BC, Canada

Lars Jorgensen
ThorCon US, Inc., Cheyenne, WY, United States; ThorCon Energy, Stevenson, WA, United States

Motoyasu Kinoshita
International Thorium Molten-Salt Forum (ITMSF), Yokohama, Japan

Esben Klinkby
Seaborg Technologies, Copenhagen, Denmark

Jan L. Kloosterman, on behalf of the SAMOSAFER consortium
Faculty of Applied Sciences, Department of Radiation Science and Technology, Delft University of Technology (TU Delft), Delft, The Netherlands

Kevin J. Kramer
RemarkTek, LLC, Redmond, WA, United States

Jiri Krepel
Paul Scherrer Institute, Villigen, Switzerland; Laboratory for Simulation and Modelling, Paul Scherrer Institute, Villigen, Switzerland

David LeBlanc
Terrestrial Energy, Inc., Oakville, ON, Canada

A.A. Lizin
State Research Centre—Research Institute of Atomic Reactors, Dimitrovgrad, Russia

Lelio Luzzi
Politecnico di Milano – Energy Department – Nuclear Engineering Division – CeSNEF (Enrico Fermi Centre for Nuclear Studies), Milano, Italy

Andrey A. Myasnikov
NRC "Kurchatov Institute," Moscow, Russia

Imre Pázsit
Chalmers University of Technology, Department of Physics, Division of Subatomic, High Energy and Plasma Physics, Göteborg, Sweden

Thomas Jam Pedersen
Copenhagen Atomics Company, Søborg, Denmark

Carl Perez
EXODYS Energy, New York, NY, United States

Eirik Eide Pettersen
Seaborg Technologies, Copenhagen, Denmark

Edward Pheil
EXODYS Energy, New York, NY, United States

Alessandro Pini
Politecnico di Milano – Energy Department – Nuclear Engineering Division – CeSNEF (Enrico Fermi Centre for Nuclear Studies), Milano, Italy

Leonid I. Ponomarev
A.A. Bochvar High-Technology Scientific Research Institute for Inorganic Materials, Moscow, Russia

Federico Puente-Espel
Seaborg Technologies, Copenhagen, Denmark

Magdi Ragheb
University of Illinois at Urbana-Champaign, Champaign, IL, United States

Jean C. Ragusa
Department of Nuclear Engineering, Texas A&M University, College Station, TX, United States

Cyril Rodenburg
Terrestrial Energy, Inc., Oakville, ON, Canada

Götz Ruprecht
Institute for Solid-State Nuclear Physics, Berlin, Germany

Andrei Rykhlevskii
Argonne National Laboratory, Lemont, IL, United States

Laszlo Sajo-Bohus
Universidad Simon Bolivar, Caracas, Venezuela, and Alba Regia Technical Faculty Obuda University, Szekesfehervar, Hungary

Toshinobu Sasa
Japan Atomic Energy Agency, Tokai, Japan

Raluca Scarlat
University of California, Berkeley, CA, United States

Andreas Vigand Schofield
Seaborg Technologies, Copenhagen, Denmark

Troels Schønfeldt
Seaborg Technologies, Copenhagen, Denmark

Ian Scott
Moltex Energy, London, United Kingdom

Christopher Taylor
Fontana Corrosion Center, Department of Materials Science and Engineering, The Ohio State University, Columbus, OH, United States; DNV GL, Oslo, Norway

S.V. Tomilin
State Research Centre—Research Institute of Atomic Reactors, Dimitrovgrad, Russia

Jan Uhlíř
Research Centre, Řež, Husinec – Řež, Czech Republic

Hector Rene Vega-Carrillo
Unidad Academica de Estudios Nucleares de la Universidad Autonoma de Zacatecas, Zacatecas, Mexico

E.P. Velikhov
Kurchatov Institute, Moscow, Russia

Daniel Weißbach
Institute for Solid-State Nuclear Physics, Berlin, Germany

Ritsuo Yoshioka
International Thorium Molten-Salt Forum (ITMSF), Yokohama, Japan

CHAPTER 6

Thermal hydraulic analysis of liquid-fueled molten salt reactors

Antonio Cammi[1], Valentino Di Marcello[2], Alessandro Pini[1] and Lelio Luzzi[1]
[1]Politecnico di Milano – Energy Department – Nuclear Engineering Division – CeSNEF (Enrico Fermi Centre for Nuclear Studies), Milano, Italy
[2]National Institute for Nuclear Physics – Gran Sasso National Laboratory (LNGS), Assergi, Italy

Contents

6.1 Introduction 263
6.2 Preliminary approach to thermohydraulics of internally heated molten salts 265
  6.2.1 Analytic framework for validation purposes 265
  6.2.2 Laminar flow 267
  6.2.3 Turbulent flow 267
6.3 Heat transfer and pressure losses 269
  6.3.1 Laminar flow 272
  6.3.2 Turbulent flow 273
6.4 Effects of internal heat generation on natural circulation stability 276
6.5 Conclusions 283
Acknowledgments 284
Abbreviations 284
References 284

6.1 Introduction

Liquid-fueled[1] molten salt reactors (MSRs) are usually considered nonclassical reactor types because of the specific nature of the fuel, which is typically constituted by a molten fluoride salt mixture circulating in the primary circuit. The fission material (uranium and/or transuranium elements) is dissolved in the molten salt carrier, which also acts as coolant. Thanks to the potentialities of this liquid fuel, several MSR concepts were investigated

[1] Solid-fueled MSRs are not considered in this chapter since they are featured by different thermo-hydraulic issues, the molten salt acting only as coolant.

Molten Salt Reactors and Thorium Energy
DOI: https://doi.org/10.1016/B978-0-323-99355-5.00003-3

at Oak Ridge National Laboratory in the past (see http://www.energyfromthorium.com/pdf/), and in recent years, MSRs have been the subject of renewed interest in the framework of Generation IV nuclear reactors (GIF, 2002, 2020; Serp et al., 2014; IRSN, 2015). These concepts differ mainly by neutron balance (critical or subcritical), neutron spectra (thermal, epithermal, or fast), the presence/absence of the graphite matrix as moderator, and the fuel salt chemical composition.

The physics of circulating nuclear fuels involves a strong coupling between neutronics and thermo-hydrodynamics, which would require in general the adoption of a multiphysics modeling approach (e.g., see, Luzzi et al., 2012b; Aufiero et al., 2014; Ramzy et al., 2020; Tiberga et al., 2020; Wan et al., 2020, and also Chapter 4.2, "Molten salt reactor multiphysics coupling and reduced order modeling", as well as Chapter 25, "Dual-fluid reactor" of this book). However, in this chapter, analyses are performed assuming that the neutronic term is decoupled from fluid dynamics and appears like a heat source within the fuel/coolant molten salt. The aim is to investigate only the thermo-hydrodynamic behavior. Reference is made to a simple axial-symmetric cylindrical geometry representative of a typical graphite-moderated MSR power channel, taking into account the thermodynamic and transport properties of the molten salt as well as its local flow conditions and heat transfer. Even if this assumption simplifies the equations to be solved, the thermo-hydrodynamic behavior of the molten salt remains complex. In this context, a preliminary analytic approach (Di Marcello et al., 2008; Luzzi et al., 2010) to evaluate the temperature radial profile in both fuel and graphite is reported in Sections 6.2 and 6.3, which are intended to offer the reader a useful validation framework for testing more sophisticated computer codes, in view of their adoption for more realistic and complex 3-D geometry analyses.

The circulating "already molten" fuel offers positive peculiarities to be exploited in the safety approach as well as in the fuel cycle of liquid-fueled MSRs (LeBlanc, 2010; Luzzi et al., 2012a; Křepel et al., 2014; Qiu et al., 2016; Chisholm et al., 2020; Pathirana et al., 2021). For instance, the fluid nature of the fuel means that the reactor core meltdown is an irrelevant instance. Moreover, the reactor has almost no excess of nuclear reactivity, which reduces the risk of accidental reactivity insertion. On the contrary, the decay heat produced by the liquid fuel dissolved into the molten salt and distributed along a closed loop may impair the natural circulation features, leading to undesired behavior of the reactor. Actually, natural circulation in the presence of internal heat generation (IHG) is characterized by a particular dynamics that needs to be carefully studied. In this context, Section 6.4 presents a preliminary investigation of IHG effects on natural circulation with reference to the stability maps of single-phase rectangular loops.

6.2 Preliminary approach to thermohydraulics of internally heated molten salts

This section presents a preliminary approach to the thermohydraulics of internally heated molten salts useful to assess and compare the numerical solutions achievable by different computer codes. For the computational fluid dynamics (CFD) analyses, we have chosen two software packages: COMSOL Multiphysics as the finite element software and ANSYS FLUENT (referred to as FLUENT throughout the rest of the chapter) as the finite volume software. The validation framework adopts the well-established analytic solution of flow in long smooth pipes, both in laminar and turbulent regimes, and has been set up in analogy with other works performed for innovative reactors, like the supercritical water reactor (Yang et al., 2007; Cervi and Cammi, 2018) and the accelerator-driven system (Cheng and Tak, 2006). It can be also an "excellent building-block case for testing turbulence models" (Wilcox, 2006), but such investigation is outside the scope of the present section.

6.2.1 Analytic framework for validation purposes

We refer to the analytic solution of the radial temperature profile, in the presence of a volume-heat source within the fluid, for a circular-pipe system in cylindrical coordinates (r, θ, z) in the case of both laminar and turbulent flow. The solution was found by Poppendiek (1954) under the following assumptions:

- Axial-symmetric conditions are taken into account.
- Thermal and hydrodynamic patterns are established (long pipes).
- Fluid axial conduction is neglected.
- Steady state exists.
- Uniform volume-heat source exists within the fluid.
- Physical properties are not a function of temperature.
- Heat is transferred uniformly to or from the fluid at the pipe wall.
- In the case of turbulent flow, an analogy exists between heat and momentum transfer.

Under the above assumptions, the differential Eq. (6.1) and the boundary conditions in Eqs. (6.2) and (6.3) describing the heat transfer in the pipe system for laminar or turbulent flow can be written according to the following 1-D formulation:

$$\frac{d}{dr}\left[(\alpha+\varepsilon)r\frac{dT(r)}{dr}\right]=\frac{u(r)}{u_m\rho c_P}\left[q'''-\frac{2}{r_0}q''_W\right]r-\frac{q'''r}{\rho c_P} \tag{6.1}$$

$$q''_W=-\lambda(dT/dr)|_{r=r_0} \tag{6.2}$$

$$T(r=r_D)=T_D \tag{6.3}$$

where T is the fluid temperature, function of the radial coordinate r; α, λ, ρ, and c_P are the thermal diffusivity, the thermal conductivity, the density, and the specific heat capacity of the fluid, respectively; ε is the fluid eddy diffusivity, function of both the radial coordinate and the axial component of the fluid velocity $u(r)$; u_m is the mean fluid velocity; r_0 is the pipe radius; q''' and q''_W are the volume-heat source and the uniform wall-heat flux, respectively. The second boundary condition, expressed by Eq. (6.3), is some reference temperature T_D such as wall, center-line, or mixed-mean fluid temperature (r_D being the radial coordinate at which T_D is evaluated).

As far as CFD simulations are concerned, steady-state conditions are considered with reference to a 2-D axial-symmetric (r,z) computational domain. It is assumed that the fluid is incompressible, homogeneous, and its physical properties are not a function of temperature. Moreover, the action of gravity is neglected. For the analyses in turbulent regime, the standard $k-\varepsilon$ model has been selected, which is the two-equation model most widely used as a reference among the several turbulence models available in the literature (Pope, 2000; Wilcox, 2006; Davidson, 2015).

As for the modeling of the near-wall region, in the COMSOL simulations we have adopted the *logarithmic wall-functions*, assuming that the computational domain begins at a certain distance, which depends on the mesh size, from the real wall. Instead, for FLUENT calculations, the *enhanced wall treatment* approach has been chosen.

Great effort was spent in setting up the mesh elements/cells size, particularly at walls and interfaces, by means of a mesh sensitivity analysis that is not reported here for brevity. It must be noted that, even for the simple circular-pipe geometry herein adopted as validation framework, the accuracy of numerical results depends on the fluid properties, the meshing strategy, and the turbulence model, as clearly demonstrated by analogous studies performed for other fluids in the same geometry (Cheng and Tak, 2006; Yang et al., 2007; Ali et al., 2017).

Concerning the numerical strategy, the *segregated algorithm* has been used in both codes. A complete description of the fluid flow modeling and of the different available options is given in the FLUENT and COMSOL user's guides (COMSOL, 2020; FLUENT, 2021).

6.2.2 Laminar flow

The solution of the boundary-value problem defined by Eqs. (6.1−6.3) was achieved by Poppendiek (1954) in the case of laminar flow, considering that the eddy diffusivity is null in laminar regime, and the fluid velocity attains a parabolic profile along the pipe radius once the hydrodynamic pattern is established. The solution is given by Eq. (6.4):

$$\frac{T(r) - T_C}{q''' r_0^2 / 2\lambda} = \frac{2F - 1}{2}\left(\frac{r}{r_0}\right)^2 - \frac{F}{4}\left(\frac{r}{r_0}\right)^4 \tag{6.4}$$

where T_C is the center-line temperature and $F = 1 - (2q''_W / q''' r_0)$, namely {1 − fraction of heat generated within moving fluid that is transferred at wall} (El-Wakil, 1978; Todreas and Kazimi, 1990).

The dimensionless radial temperature profile given by Eq. (6.4) is plotted in Fig. 6.1 for several values of the function F and is compared with the CFD simulation results obtained by means of COMSOL and FLUENT. As can be noticed, both numerical solutions are practically superimposed on the analytic one.

6.2.3 Turbulent flow

For the case of turbulent flow, the boundary-value problem defined by Eqs. (6.1−6.3) can be separated into the following two simpler boundary-value problems, whose solutions can be superimposed to yield the solution of the "original problem":

1. A problem representing a flow system with a volume-heat source, but with no wall-heat flux.
2. A problem representing a flow system without a volume-heat source, but with a uniform wall-heat flux.

The solution for problem (1) was found by Poppendiek (1954) with the following procedure. At first, the radial heat flux profile is calculated assuming that the velocity profile may be satisfactorily represented by two regions

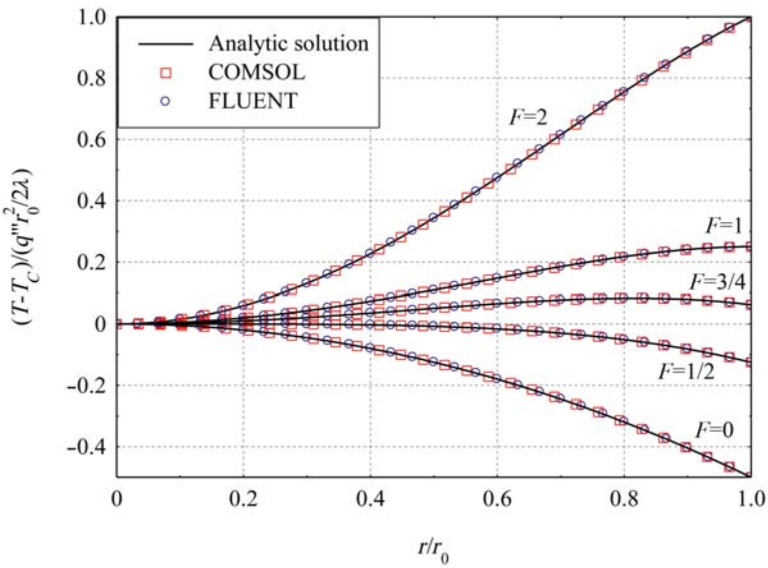

Figure 6.1 Comparison between the different evaluations of the dimensionless radial temperature profile in a pipe with laminar flow.

(a laminar layer and a turbulent core with the so-called "venerable" one-seventh power law for the velocity; see Nikuradse, 1950; Todreas and Kazimi, 1990; De Chant, 2005). Therefore, the radial heat flux is replaced with simple monomials and polynomials and is integrated layer by layer (laminar sublayer, buffer layer, outer turbulent layer, and inner turbulent layer) to find the radial temperature profile. The dimensionless radial temperature profile turns out to be a function of both Reynolds (*Re*) and Prandtl (*Pr*) numbers (Martinelli, 1947; Poppendiek, 1954).

The solution for problem (2) was originally found by Martinelli (1947) assuming three layers (laminar sublayer, buffer layer, and turbulent layer) for the calculation of both the velocity and the temperature profiles. It is worth mentioning that in the buffer and turbulent layer, Martinelli preferred a logarithmic law for the velocity based on experimental data (i.e., the so-called generalized velocity profile). In this work, we follow an alternative analytic solution based on the same approach of Poppendiek, briefly described above for problem (1), adopting the one-seventh power law for the velocity and the same four layers of Poppendiek for the radial temperature. The comparison between the Martinelli and this work approaches is shown in Fig. 6.2 in terms of the temperature difference with respect to the center-line pipe temperature as a function of the

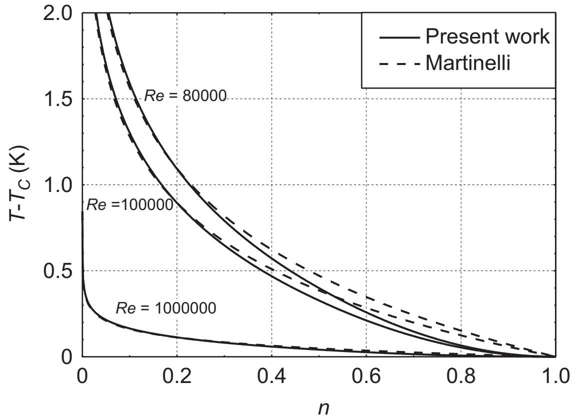

Figure 6.2 Comparison between the different evaluations of the radial temperature profiles in a pipe with turbulent flow for several Reynolds numbers and $Pr=1$ – problem (2).

dimensionless distance n from the pipe wall ($n \equiv 1-r/r_0$). The two approaches substantially agree with little differences at lower Reynolds numbers and in the center of the pipe.

The temperature profile of the "original problem" can be easily achieved by superimposing the temperature profiles of problems (1) and (2). In Fig. 6.3, results of the CFD analyses for the "original problem" are compared with the analytical ones achievable following the Martinelli and this work approaches for the problem (2).

The numerical results in terms of velocity (Fig. 6.3A) and temperature (Fig. 6.3B) profiles follow very well those provided by both analytic approaches, which are very close to each other.

As for the velocity, numerical results provided by both codes are in good agreement, whereas the analytical profiles show some little differences due to the modeling assumptions (i.e., logarithmic and one-seventh laws).

As far as the temperature is concerned, it must be pointed out that a more accurate agreement can be found by means of FLUENT in the near-wall region thanks to the *enhanced wall treatment* approach of the boundary layer.

6.3 Heat transfer and pressure losses

In graphite-moderated MSRs, a notable characteristic is that while the energy from nuclear fission reactions is primarily released directly in the

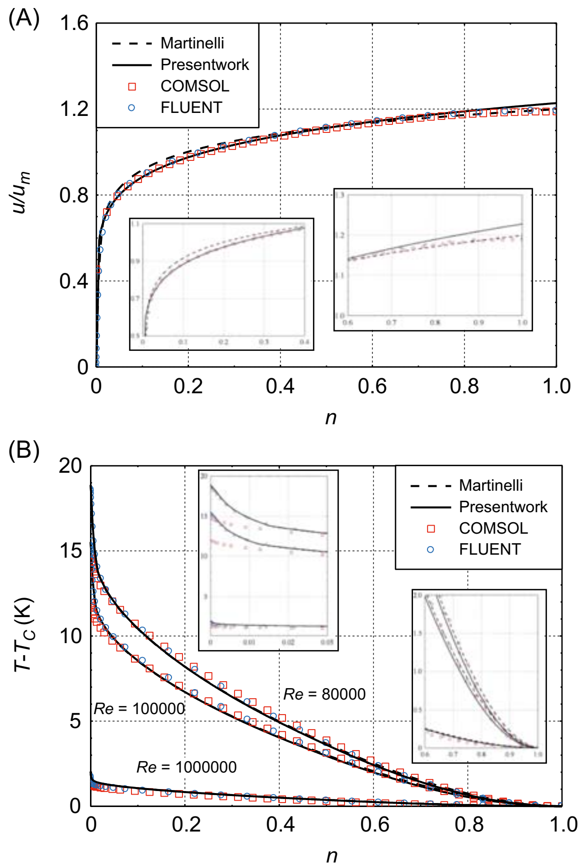

Figure 6.3 Comparison between the different evaluations of (A) the dimensionless velocity profile, and (B) of the radial temperature profile in a pipe with turbulent flow for several Reynolds numbers and $Pr = 1$ – "original problem" = (1) + (2).

fuel, the graphite channels experience heating from gamma and neutron radiation. This additional heat source often leads to a radial temperature gradient from the fuel towards the graphite. In other words, the liquid fuel practically cools down the graphite in steady-state operation (Křepel et al., 2005; Křepel et al., 2007).

The investigation of the heat exchange properties between molten salt and graphite is performed with reference to an axial-symmetric geometry representing a typical MSR core channel, idealized as a circular pipe with circulating molten salt that is surrounded by a hollow cylinder of graphite.

By coupling the analytic approach described in Section 6.2 for modeling the fully developed flow of molten salt inside the pipe with the heat conduction problem for the graphite, it is possible to find the radial temperature profile in the channel (graphite + molten salt). The previous solutions (1) and (2) can be used for the molten salt, while for the graphite the following radial profile is obtained by solving the 1-D heat conduction equation between the inner (R_i) and the outer (R_o) radii of graphite:

$$T(r) = \frac{q'''_g}{2\lambda_g}\left(\frac{R_i^2 - r^2}{2} + R_o^2 \ln\left(\frac{r}{R_i}\right)\right) + T_W \tag{6.5}$$

where q'''_g and λ_g are the volume-heat source and the thermal conductivity of the graphite, and T_w is the interface molten salt-graphite temperature. The heat flux at the interface, q''_W, is given by Eq. (6.6):

$$q''_W = -q'''_g(R_o^2 - R_i^2)/2R_i \tag{6.6}$$

To calculate the wall temperature T_W, it is necessary to first solve the heat transfer problem in the molten salt. This involves applying the wall heat flux given by Eq. (6.6) as a boundary condition, and specifying the values of the volume-heat source in both the molten salt (q'''_s) and the graphite (q'''_g). In the next analyses, a ratio q'''_g/q'''_s of about 3% is adopted (Mandin et al., 2005).

Once the radial temperature profile is known, it is possible to calculate analytically the Nusselt number as $Nu = (D_h/\lambda) \cdot q''_W/(T_W - T_b)$ and consequently the heat transfer coefficient between the molten salt and the graphite as $h = Nu \cdot \lambda/D_h$, where T_b and D_h are the bulk (or mixed-mean) temperature of the molten salt and the channel hydraulic diameter, respectively.

It must be pointed out that in the case of heat source within the fluid, the Nusselt number is not only a function of Reynolds and Prandtl numbers but also of the ratio between the heat source and the wall heat flux (Poppendiek, 1954; Fiorina et al., 2014).

Two different cases are considered for the CFD analyses: (I) no volume-heat source within the molten salt and (II) molten salt with volume-heat source. The first case (whose results are shown for both the laminar and the turbulent flow) is important not only for the above statement about the Nusselt number but also because heat transfer properties of molten salt are of interest for its usage in the intermediate-heat exchanger (Mandin et al., 2005).

Table 6.1 Main reference data of the analyzed molten salt reactor channel.

Symbols/quantities	Molten salt	Graphite
c_P, specific heat capacity [J/kg · K]	1357	1760
D_h, channel hydraulic diameter [m]	0.16	—
H, channel length [m]	4.8	4.8
Pr, Prandtl number [−]	11	—
q''', volume-heat source [W/m^3]	$1.3 \cdot 10^8$	$3.4 \cdot 10^6$
R_i, interface radius [m]	0.08	0.08
R_o, outer radius [m]	—	0.12
T_{in}, channel inlet temperature [K]	900	—
η, dynamic viscosity [kg/m · s]	0.01	—
λ, thermal conductivity [W/m · K]	1.23	31.2
ρ, density [kg/m^3]	3330	1843

The second case is more representative of an MSR core channel, and the respective results are shown for brevity only in turbulent flow, which is expected to occur during reactor operating conditions. For what concerns molten salt and graphite properties, MSR design specifications, and the volume-heat sources, we refer to Mandin et al. (2005), while the most important data are summarized in Table 6.1.

6.3.1 Laminar flow

A Reynolds number $Re = 80$ is chosen for this analysis, referring to the case with no volume-heat source within the molten salt. In Fig. 6.4, the local Nusselt number achieved by the CFD simulations (considering a length of 15 m in order to reach fully developed flow conditions) is compared with the following correlation given by Bird et al. (1960), which is valid for thermally developing flow with constant wall heat flux:

$$Nu_z = \begin{cases} 1.302(z^*)^{-1/3} - 1.0 & \text{for } z^* \leq 5 \cdot 10^{-5} \\ 1.302(z^*)^{-1/3} - 0.5 & \text{for } 5 \cdot 10^{-5} \leq z^* \leq 1.5 \cdot 10^{-3} \\ 4.364 + 8.68\left(10^3 \cdot z^*\right)^{-0.56} \cdot \exp(-41 \cdot z^*) & \text{for } z^* \geq 1.5 \cdot 10^{-3} \end{cases} \tag{6.7}$$

where $z^* = z/(Re \cdot Pr \cdot D_h)$. COMSOL and FLUENT codes supply the same results, which are in very good agreement with the correlation given by Bird et al. as well as with the analytical evaluation of the local Nusselt number (see also Table 6.2). The friction pressure losses are numerically evaluated considering a parabolic profile of the inlet velocity and are

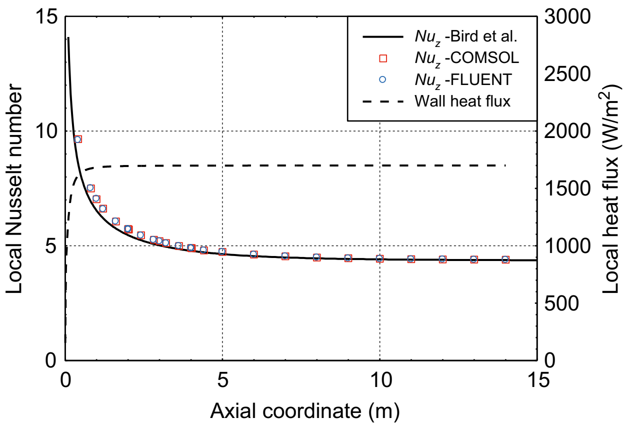

Figure 6.4 Comparison between the different evaluations of the local Nusselt number in the molten salt reactor channel with laminar flow.

Table 6.2 Comparison between analytic and numerical calculations of the local *Nu* and friction pressure losses in the MSR channel with laminar (fully developed) flow.

	Analytic	**COMSOL**	**Err (%)**	**FLUENT**	**Err (%)**
Local *Nu* (z = 13 m), [−]	4.364	4.393	0.7	4.389	0.6
Pressure losses (z = H), [Pa]	$9.00 \cdot 10^{-2}$	$8.99 \cdot 10^{-2}$	0.1	$8.97 \cdot 10^{-2}$	0.3

compared in Table 6.2 with the classical Darcy formula for the friction coefficient f in the Hagen-Poiseuille flow (i.e., $f = 64/Re$). As can be noticed, a very good agreement exists.

6.3.2 Turbulent flow

A Reynolds number $Re = 8 \cdot 10^4$ is chosen for the turbulent flow. In this subsection, the effect of the *standard k*-ω turbulence model is also investigated, and results are compared to the analytic solution and those obtained with the *standard k-ε model* for both the considered cases (I) and (II). For the numerical simulations, COMSOL and FLUENT codes have been adopted. Radial temperature profiles are shown in Fig. 6.5, while the Nusselt number and the friction pressure losses calculations are given in Tables 6.3 and 6.4, respectively.

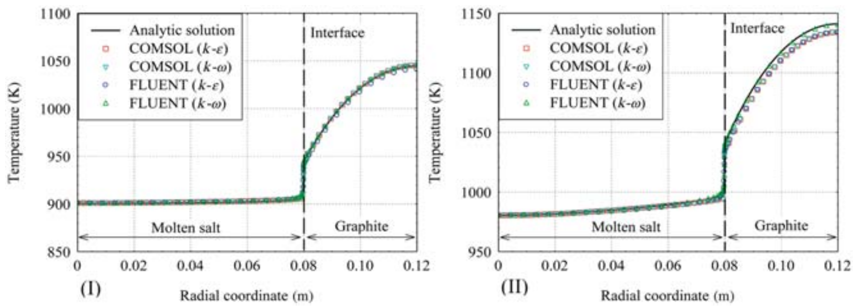

Figure 6.5 Comparison between the different evaluations of the temperature profile in the molten salt reactor channel with turbulent flow ($z = 4.4$ m): (I) without, and (II) with volume-heat source.

Table 6.3 *Nu* comparison with the analytic solution in the MSR channel (turbulent flow).

Local *Nu* ($z = 4.4$ m)	Case (I)	Err (%)	Case (II)	Err (%)
Analytic solution	523	–	418	–
Dittus-Boelter correlation	502	4.0	502	20
COMSOL k–ε	512	2.1	474	13
COMSOL k–ω	517	1.2	472	13
FLUENT k–ε	584	12	469	12
FLUENT k–ω	526	0.7	422	1.1

Table 6.4 Pressure losses comparison with the McAdams correlation in the molten salt reactor channel for the turbulent flow ($z = H$).

Friction pressure losses	[Pa]	Err (%)
McAdams correlation	2163	–
COMSOL k–ε	2021	6.6
COMSOL k–ω	2036	5.9
FLUENT k–ε	2332	7.8
FLUENT k–ω	2193	1.4

As a result, there is good agreement of the numerical evaluations of both the Nusselt number and the temperature profiles with those obtained analytically. The well-known Dittus-Boelter correlation can be used for molten salt (El-Wakil, 1978; Todreas and Kazimi, 1990; Mandin et al., 2005) giving a reasonable result in the case of no heat source with a discrepancy of 4% in comparison with the analytic solution, but it should be used carefully in the presence of a heat source within the fluid because it does not take into account the dependence of heat transfer on the ratio between wall heat flux and volume-heat source. As a consequence, the heat transfer coefficient could be excessively overestimated (see Table 6.3). This last issue has been the subject of several works (e.g., Di Marcello et al., 2010; Luzzi et al., 2010, 2012a; Fiorina et al., 2014) to which the reader is referred. Here, we just retrieve from Fiorina et al. (2014) an example concerning the core channels of the molten salt breeder reactor (Robertson, 1971). As can be noticed in Fig. 6.6, traditional correlations (Dittus and Boelter, 1930; Sieder and Tate, 1936; Gnielinski, 1976; Bin et al., 2009; Yu-ting et al., 2009) predict a higher Nusselt number compared to the correlation proposed by Di Marcello et al. (2010) that takes into account the volume-heat source in the molten salt. This leads to an underestimation of the graphite temperature, whose importance depends also on the channel diameter and the strength of heat source in the fuel.

A good agreement can be found between the numerical evaluations of the pressure losses and the well-known McAdams correlation (see Table 6.4).

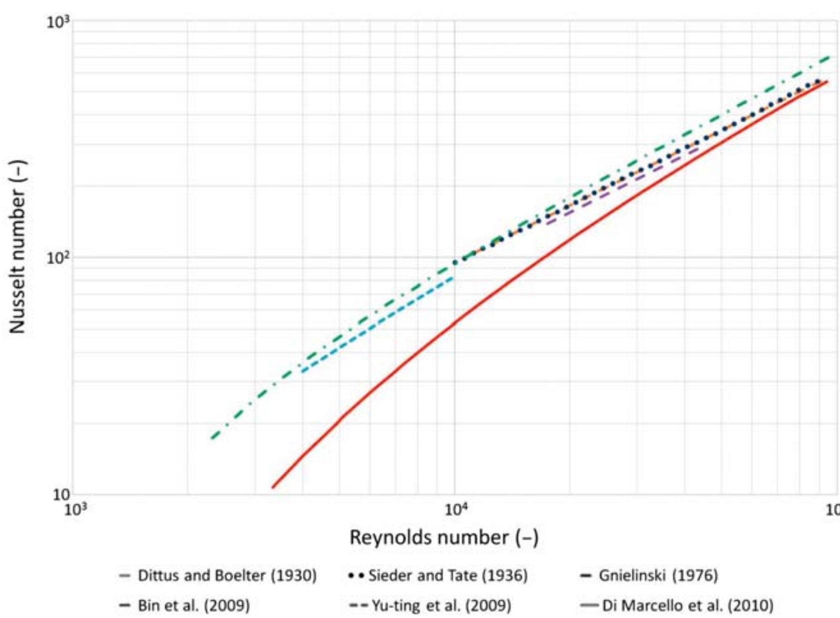

Figure 6.6 Nusselt number in the core channels of the molten salt breeder reactor.

As a general comment on the analyses presented in this section, we can observe that the numerical results provided by COMSOL and FLUENT codes are close to each other in terms of temperature profiles, Nusselt number, and pressure losses. Some differences have been found, which are related to the choice of different turbulence models, but it is not the aim of this chapter to enter into such details. Moreover, the influence of the volume-heat source on the heat transfer properties may be relevant at low Reynolds numbers and needs to be carefully taken into account.

6.4 Effects of internal heat generation on natural circulation stability

Analytical, numerical, and experimental studies on the stability and transient behavior of single-phase natural circulation loops (NCLs) have been performed in recent years by several authors. An overview can be found in Misale (2014). However, all these works performed the analysis of NCLs with localized hot and cold heat sinks, mainly focusing on the influence of the loop geometry on natural circulation instabilities, while the instance of an internal and distributed power source inside the system has been little investigated. In this regard, the first studies have been conducted by Pini et al. (2014), Ruiz et al. (2015), Pini et al. (2016), Cammi et al. (2016b), Cammi et al. (2017), Luzzi et al. (2017), and Battistini et al. (2021). Referring the reader to these two studies for a detailed description of the methods developed for the stability analysis, as well as of the main modeling assumptions adopted, hereafter the main results are summarized. They are expressed in terms of dimensionless stability maps, which are a compact way to describe the dynamic behavior of a given system.

Reference is made to the two vertical loop configurations with constant diameter D shown in Fig. 6.7 that can be characterized by large instability regions, namely the HHHC (horizontal heater—horizontal cooler) and the VHHC (vertical heater—horizontal cooler) loops.

Their geometrical features (Vijayan et al., 2007) are given in Table 6.5. A single cooling section (called *cooler*) is considered and is modeled as a constant wall temperature heat exchanger, while two heat sources can be taken into account. The first is a localized external heater (called *heater*) and is treated as a localized heat flux (LHF) source, q''. The second represents the heat generation inside the fluid (e.g., the circulating fuel in MSRs) and is modeled as a homogeneous distributed

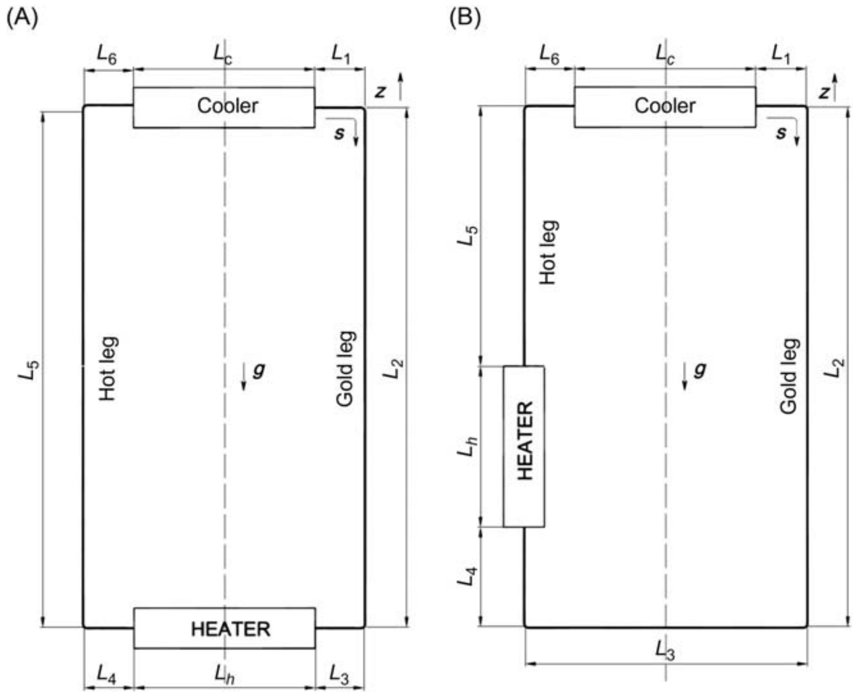

Figure 6.7 Rectangular loop configurations: (A) horizontal heater—horizontal cooler; (B) vertical heater—horizontal cooler (not to scale).

Table 6.5 Dimensions (in meters) of the horizontal heater—horizontal cooler and vertical heater—horizontal cooler loops.

Loop	L_1	L_2	L_3	L_4	L_5	L_6	Lc	Lh	Lt	D
HHHC	0.31	2.20	0.40	0.40	2.20	0.31	0.80	0.62	7.24	0.0269
VHHC	0.31	2.20	1.42	0.35	1.12	0.31	0.80	0.73	7.24	0.0269

volumetric source[2], q'''. The fluid flow is considered one-dimensional along the curvilinear coordinate s (adopted to describe the position

[2] In MSRs, the heat production inside the fluid takes place through fission reactions in the reactor core and through nuclear decays of the fission products in the whole primary circuit. However, the decay heat variation along the primary circuit is small. The strongest heat release takes place inside the core (or at the core exit, when it is generated by the fastest decaying fission products). After the core shutdown, during an emergency condition, the decay heat along the primary circuit can be considered uniform.

inside the loop), and it is assumed that the same flow regime (laminar, laminar turbulent transition, or fully turbulent) exists in the whole loop.

For comprehension of the stability maps, which are obtained by perturbing the system equilibrium, the following steady-state quantities are to be defined: the temperature variation due to the external heat flux in the heater section ($\Delta Tq''$) and the temperature variation of the fluid induced by the internal generation outside the cooler ($\Delta Tq'''$):

$$\Delta T_{q''} = \frac{q''(P/A)}{G_0 C_p} L_h \tag{6.8}$$

$$\Delta T_{q'''} = \frac{q'''}{G_0 C_p}(L_t - L_c) \tag{6.9}$$

where G_0 is the mass flux, Cp is the fluid reference specific heat (taken at the cooler entrance), P and A are the perimeter and the cross-section area of the pipes, respectively, L_h is the heater length, L_c is the cooler length, and L_t is the total length of the loop. At this point, it is also possible to define the total temperature variation outside the cooler (ΔT_{tot}), the ratio α between $\Delta T_q''$ and ΔT_{tot}, and the modified Stanton number (St_{m0}):

$$\Delta T_{tot} = \Delta T_{q''} + \Delta T_{q'''} \tag{6.10}$$

$$\alpha = \frac{\Delta T_{q''}}{\Delta T_{\mathrm{tot}}}(0 \le \alpha \le 1) \tag{6.11}$$

$$St_{m0} = 4St_0 \frac{L_t}{D} = 4\frac{Nu_0}{Re_0 Pr_0}\frac{L_t}{D} = \frac{h_0(P/A)}{G_0 C_p} L_t \tag{6.12}$$

where St_0 is the Stanton number, Nu_0 is the Nusselt number, Re_0 is the Reynolds number, Pr_0 is the Prandtl number, h_0 is the convective heat transfer coefficient, and the subscript 0 indicates steady-state values. The α ratio can assume all values between 0 and 1. For $\alpha = 1$, there is only the localized external heat source (*conventional* natural circulation). For $\alpha = 0$, only a homogeneously distributed IHG is present in the system. An example of steady-state distribution, both for $\alpha = 1$ and $\alpha = 0$, is shown in Fig. 6.8. This parameter has a great influence on the NCL dynamic behavior, because a variation of α directly implies a change in the ratio between the heat produced by the LHF in the heater and the distributed

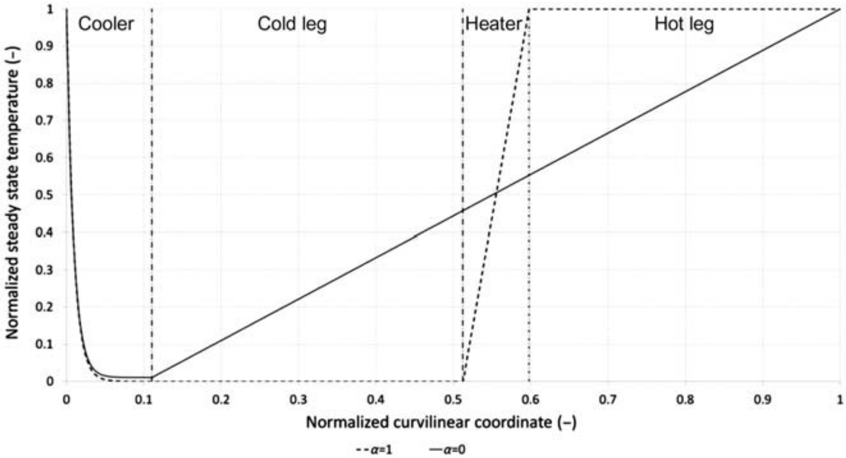

Figure 6.8 Horizontal heater–horizontal cooler loop: steady-state temperature field for $\alpha = 0$ (internal generation only) and $\alpha = 1$ (conventional natural circulation).

IHG. When α is changed, the same system can experience stable or unstable natural circulation flow regimes. Actually, as will be shown, the stability maps strongly depend on α.

Another important parameter, generally not considered in the literature, but affecting the dynamic behavior of the system as well, is herein denoted B. It reads:

$$B = \frac{G_0}{h_0}\left(\frac{\partial h}{\partial G}\right)_0 \tag{6.13}$$

The parameter B has been evaluated in Pini et al. (2016), to which we refer for details, and has the trend shown in Fig. 6.9 for different values of the Prandtl number. It represents the variation of convective heat transfer coefficient due to mass flux perturbations. If B is equal to zero, this relation is not taken into account, and the heat transfer coefficient h is treated as a fixed parameter at the steady state value (h_0), by neglecting its dependence on the mass flow rate (and hence on the Reynolds number).

Given the above definitions of the α and B parameters, we can now summarize some significant results in terms of stability maps for the two considered loop configurations. Natural circulation may occur at different flow regimes, from the laminar to the turbulent, depending on the thermal power given to the system. The steady-state condition is reached when a dynamic equilibrium is established between the buoyancy and the

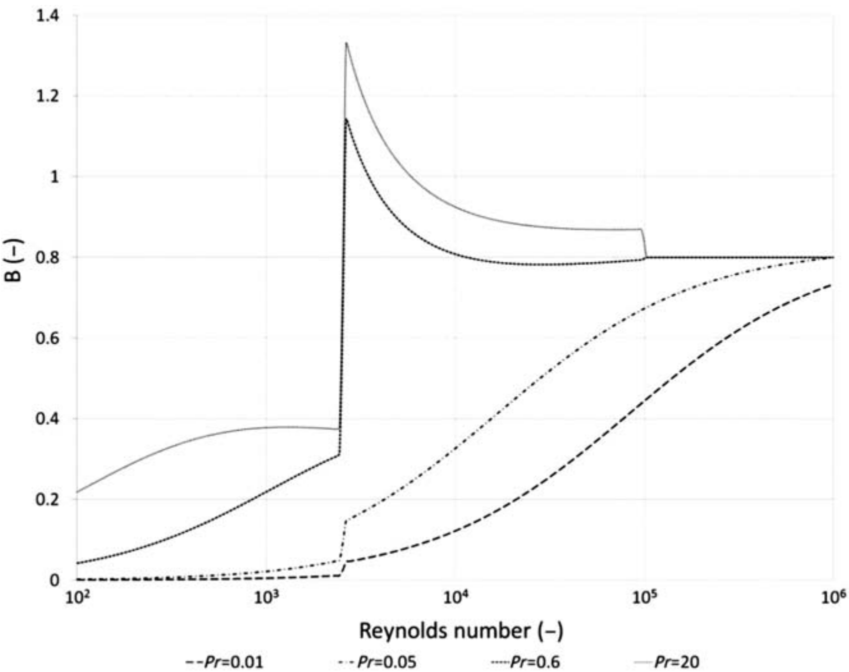

Figure 6.9 Trend of *B* with respect to the Reynolds and the Prandtl numbers.

frictional effects. This equilibrium can be stable or unstable. In the last case, the instabilities can lead to large pulsations in the fluid flow rate and unwanted behavior of the system. For a given loop configuration and a given value of α, in a *Re* versus St_{mo} diagram, the geometrical locus of the points for which the mass flux remains constant (after the perturbation of the steady state) sets a boundary separating the couples (Re_0, St_{m0}) for which the equilibrium is asymptotically stable from those for which the equilibrium is unstable. This is the definition of the stability map.

As already mentioned, IHG can significantly modify the dynamic behavior of natural convection loops. Fig. 6.10 shows the stability maps of the HHHC and VHHC systems for $B=0$ (fixed heat transfer coefficient), from $\alpha=1$ (only localized external heating) to $\alpha=0$ (only IHG). As can be noticed, the unstable regime increases when IHG is present.

The HHHC loop configuration represents a very critical situation since, for any value of α, it always remains a symmetric system (see Fig. 6.7A), and therefore the fluid does not have any preferable flowing direction. When $B \neq 0$ (see Fig. 6.11A), the heat exchange varies with the mass flux perturbation and induces a strong stabilization. This effect is

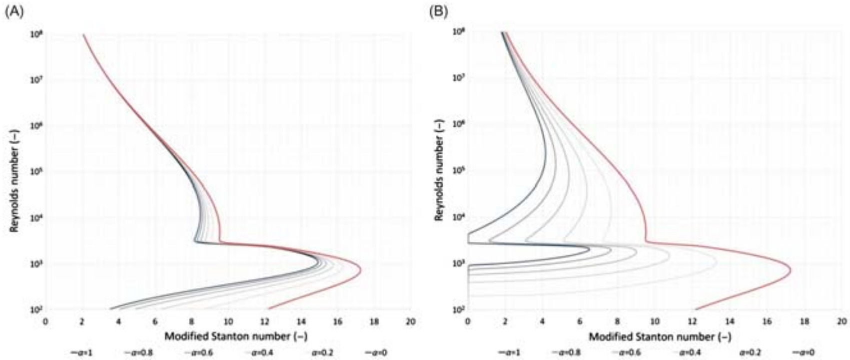

Figure 6.10 Stability maps of horizontal heater–horizontal cooler (A) and vertical heater–horizontal cooler (B) loops for various internal heat generation levels. The effect of heat exchange is neglected ($B = 0$). Stable and unstable regions are on the right and on the left of the curves, respectively.

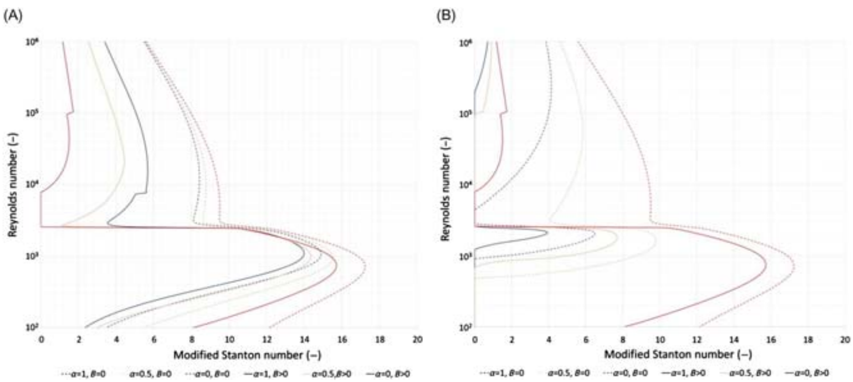

Figure 6.11 Stability maps of horizontal heater–horizontal cooler (A) and vertical heater–horizontal cooler (B) loops with ($B \neq 0$) and without ($B = 0$) the effect of heat exchange, for different internal heat generation levels. Stable and unstable regions are on the right and on the left of the curves, respectively.

larger in the range of Reynolds numbers for which the value of B is higher (see Fig. 6.9). Moreover, the stabilization becomes stronger as the fraction of the power given by the internal generation increases (from $\alpha = 1$ to $\alpha = 0$). Since the influence of the volumetric heat generation is small, the effect of B is able to reverse the stability behavior of the system for laminar-turbulent transition and fully turbulent zones (where B is bigger compared to the laminar zone, as Fig. 6.9 shows). Hence, the system is more stable for $\alpha = 0$ than for $\alpha = 1$ when $Re > 2500$.

The behavior of the VHHC configuration is completely different with respect to the previous case. As a matter of fact, when the power is given by the localized heater ($\alpha = 1$), the flow has a preferred direction for its motion, that is the clockwise one (see Fig. 6.7B). On the contrary, as α becomes zero, the loop progressively acquires a symmetric configuration, and hence, the system becomes more unstable. The destabilization induced by the IHG is so marked (see Fig. 6.10B) that the case of $\alpha = 0$ remains the most unstable also considering the heat exchange effect (see Fig. 6.11B).

Fig. 6.11 clearly shows that the overall effect of the B parameter is that of stabilizing the system dynamics. This can be explained as follows. If the mass flux oscillations increase, the convective heat transfer in the cooler is enhanced. Since the power given to the system is constant, when the heat exchange increases, the mean temperature difference between hot and cold legs of the loop becomes smaller. The final consequence of this mechanism is the weakening of the buoyancy force, which is induced by the density variation caused by the nonuniform temperature field.

To summarize, it has been found that IHG combined with heat exchange effect can induce a stabilization or a destabilization of the system dynamics depending on its action on the loop symmetry. For the HHHC loop, which presents a perfect axial symmetry for every value of α, IHG together with the heat transfer phenomena induces stabilization. On the other hand, for the VHHC loop, which does not have any symmetry for $\alpha = 1$, IHG combined with the heat exchange effect causes a destabilization because it increases the symmetry of the loop. By considering the two effects in a separate way, the heat exchange ($B \neq 0$) acts on the system oscillations with a negative feedback, whose influence increases as the fluid IHG becomes larger. On the contrary, the volumetric power source destabilizes the system.

We believe that it is fundamental to validate the predictions of the presented stability maps with experimental data. For this purpose, the DYNASTY testing facility, built at the Department of Energy (Politecnico di Milano), can give a fundamental support (Cammi et al., 2016a; Battistini et al., 2021), also providing useful information on some effects that were not discussed in this work, such as nonuniform power generation, cross-stream temperature gradients effects, and nonuniformity of the fluid parameters. The experimental campaign started in the Spring of 2022 and will conclude its first phase in 2023. The acquired knowledge will constitute the background necessary for understanding how the decay heat distributed along the primary circuit of an MSR can modify the dynamics of natural circulation, potentially leading to the dangerous behavior of the reactor. Such an occurrence needs to be carefully avoided through an appropriate design based on the outcomes of the planned investigations. In other words, the study of the dynamic behavior of natural circulation with IHG is important in order to achieve high levels of intrinsic safety, which is one of the pillars of the Generation IV International Forum.

6.5 Conclusions

In this chapter, a preliminary approach to thermohydraulics of a typical (graphite-moderated) MSR channel has been presented by assuming that the neutronic problem is decoupled from fluid dynamics and referring to a simple axial-symmetric geometry. Some relevant aspects of this system, featured by a heat source within the fuel/coolant molten salt, have been analyzed. In particular, a validation framework has been proposed in order to test different computer codes. In the presented analyses, we have adopted COMSOL and FLUENT, whose numerical results in terms of temperature profiles and pressure losses turned out to be very close to each other and substantially in good agreement with the analytical solutions and data given by empirical correlations. However, more detailed analyses are required in the case of more complex and design-oriented geometries, taking into account the effects concerning the geometry itself, the influence of the volume-heat source on the heat transfer, and the choice of both the mesh structure and the turbulence model. For this purpose, the strong coupling between neutronics and thermohydraulics, which is a specific and intrinsic feature of liquid-fueled MSRs, needs to be considered as well.

The presented results on the natural circulation stability, although preliminary, have clearly shown that the behavior in the presence of IHG is characterized by a particular dynamics. Actually, system equilibria that are asymptotically stable for NCLs with conventional LHF can become unstable when IHG is present. The stability maps have proved that IHG, when it dominates the localized external heat source, can modify the shape and area of the stability regions. These findings contribute to the development of the natural circulation modeling, introducing physical phenomena previously neglected, and suggest that IHG effects should be taken into account when designing convective loops with internally heated fluids. As far as future developments are concerned, the influence of the thermal properties of the pipe walls is currently under investigation at Politecnico di Milano, and loop configurations featured by significant 3-D effects and with different positions of the localized heater and of the cooling section will be considered as well.

Acknowledgments

We gratefully acknowledge financial support from Politecnico di Milano (FARB Project, Grant no. DDM2RIST06) for the construction of the DYNASTY testing facility.

Abbreviations

CFD	Computational fluid dynamics
DYNASTY	DYnamics of NAtural circulation for molten SalT internallY heated
HHHC	Horizontal heater−horizontal cooler
IHG	Internal heat generation
LHF	Localized heat flux
MSR	Molten salt reactor
NCL	Natural circulation loop
VHHC	Vertical heater−horizontal cooler
1-D	One-dimensional
2-D	Two-dimensional
3-D	Three-dimensional

References

Ali, Z., Tucker, P.G., Shahpar, S., 2017. Optimal mesh topology generation for CFD. Comp. Methods Appl. Mech. Eng. 317, 431−457.
Aufiero, M., Cammi, A., Geoffroy, O., Losa, M., Luzzi, L., Ricotti, M.E., et al., 2014. Development of an OpenFOAM model for the molten salt fast reactor transient analysis. Chem. Eng. Sci. 111, 390−401.
Battistini, A., Cammi, A., Lorenzi, S., Colombo, M., Fairweather, M., 2021. Development of a CFD −LES model for the dynamic analysis of the DYNASTY natural circulation loop. Chem. Eng. Sci. 237, 116520_1−13.
Bin, L., Yu-ting, W., Chong-Fang, M., Meng, Y., Hang, G., 2009. Turbulent convective heat transfer with molten salt in a circular pipe. Int. Commun. Heat. Mass. Transf. 36, 912−916.
Bird, R.B., Stewart, W.E., Lightfoot, E.N., 1960. Transport Phenomena. Wiley, New York, USA.
COMSOL, 2020. COMSOL Multiphysics® 5.6 User's Guide, COMSOL Inc., 2020.
Cammi, A., Cauzzi, M.T., Luzzi, L., Pini, A., 2016a. DYNASTY: an experimental loop for the study of natural circulation with internally heated fluids. In: Proceedings of the 12th International Conference on Heat Transfer, Fluid Mechanics and Thermodynamics, 11−13 July 2016, Malaga, Spain, pp. 1159−1164.
Cammi, A., Luzzi, L., Pini, A., 2016b. The Influence of the wall thermal inertia over a single-phase natural convection loop with internally heated fluids. Chem. Eng. Sci. 153, 411−433.
Cammi, A., Misale, M., Devia, F., Cauzzi, M.T., Pini, A., Luzzi, L., 2017. Stability analysis by means of information entropy: Assessment of a novel method against natural circulation experimental data. Chem. Eng. Sci. 166, 220−234.

Cervi, E., Cammi, A., 2018. Stability analysis of the supercritical water reactor by means of the root locus criterion. Nucl. Eng. Des. 338, 137–157.
Cheng, X., Tak, N., 2006. Investigation on turbulent heat transfer to lead-bismuth eutectic flows in circular tubes for nuclear applications. Nucl. Eng. Des. 236 (4), 385–393.
Chisholm, B.M., Krahn, S.L., Sowder, A.G., 2020. A unique molten salt reactor feature – the freeze valve system: Design, operating experience, and reliability. Nucl. Eng. Des. 368, 110803_ 1–17.
Davidson, P.A., 2015. Turbulence: An Introduction for Scientists and Engineers. Oxford University Press, UK.
De Chant, L.J., 2005. The venerable 1/7th power law turbulent velocity profile: a classical nonlinear boundary value problem solution and its relationship to stochastic processes. Appl. Math. Comput. 161, 463–474.
Di Marcello, V., Cammi, A., Luzzi, L., 2008. Analysis of thermal-hydraulic behaviour of the molten salt nuclear fuel. In: Proceedings of the International Conference Nuclear Energy for New Europe 2008, 7–11 September 2008, Portorož, Slovenia, pp. 301.1–301.10.
Di Marcello, V., Cammi, A., Luzzi, L., 2010. A generalized approach to heat transfer in pipe flow with internal heat generation. Chem. Eng. Sci. 65, 1301–1310.
Dittus, F.W., Boelter, L.M.K., 1930. Heat transfer in automobile radiators of the tubular type. 2. Univ. Calif. Publ. Eng. 443–461.
El-Wakil, M.M., 1978. Nuclear Heat Transport. American Nuclear Society, USA.
FLUENT, 2021. ANSYS Fluent User's Guide 21R12021 ANSYS Inc.
Fiorina, C., Cammi, A., Luzzi, L., Mikityuk, K., Ninokata, H., Ricotti, M.E., 2014. Thermal-hydraulics of internally heated molten salts and application to the molten salt fast reactor. J. Phys. 501.
GIF, 2002. A technology roadmap for generation IV nuclear energy systems. US DOE Nuclear Energy Research Advisory Committee and the Generation IV International Forum, Technical Report GIF-002-00.
GIF, 2020. Technology roadmap update for generation IV. Nuclear energy systems. Technical Report, Available from: <https://www.gen-4.org/gif/jcms/c_178290/gif-2020-annual-report>.
Gnielinski, V., 1976. New equations for heat and mass transfer in turbulent pipe and channel flow. Int. Chem. Eng. 16 (2), 359–367.
IRSN, 2015. Review of generation IV nuclear energy systems. Institut de Radioprotection et de Sûreté Nucléaire. Available from: <http://www.irsn.fr/EN/newsroom/News/Documents/IRSN_Report-GenIV_04-2015.pdf>.
Křepel, J., Grundmann, U., Rohde, U., Weiss, F.P., 2005. DYN1D-MSR dynamics code for molten salt reactors. Ann. Nucl. Energy. 32, 1799–1824.
Křepel, J., Grundmann, U., Rohde, U., Weiss, F.P., 2007. DYN3D-MSR spatial dynamics code for molten salt reactors. Ann. Nucl. Energy 34, 449–462.
Křepel, J., Hombourger, B., Fiorina, C., Mikityuk, K., Rohde, U., Kliem, S., 2014. Fuel cycle advantages and dynamics features of liquid fueled MSR. Ann. Nucl. Energy. 64, 380–397.
LeBlanc, D., 2010. Molten salt reactors: a new beginning for an old idea. Nucl. Eng. Des. 240 (6), 1644–1656.
Luzzi, L., Cammi, A., Di Marcello, V., Fiorina, C., 2010. An approach for the modelling and the analysis of the MSR thermo-hydrodynamic behaviour. Chem. Eng. Sci. 65 (16), 4873–4883.
Luzzi, L., Aufiero, M., Cammi, A., Fiorina, C., 2012a. Thermo-Hydrodynamics of Internally Heated Molten Salts for Innovative Nuclear Reactors. InTech, Rijeka, Croatia, pp. 119–142.

Luzzi, L., Di Marcello, V., Cammi, A., 2012b. Multi-Physics Approach to the Modeling and Analysis of Molten Salt Reactors. Nova Science Publishers, Inc, New York, pp. 1−140.

Luzzi, L., Misale, M., Devia, F., Pini, A., Cauzzi, M.T., Fanale, F., et al., 2017. Assessment of analytical and numerical models on experimental data for the study of single-phase natural circulation dynamics in a vertical loop. Chem. Eng. Sci. 162, 262−283.

Mandin, P., Belachgar, H., Nuttin, A., Picard, G., 2005. Hydrothermal modelling for the molten salt reactor design optimisation. In: Proceedings of the 11th International Topical Meeting on Nuclear Reactor Thermal-Hydraulics (NURETH-11), 2−6 October 2005, Avignon, France, pp. 227.1−227.13.

Martinelli, R.C., 1947. Heat transfer to molten metals, Trans, 69. ASME, pp. 947−959.

Misale, M., 2014. Overview on single-phase natural circulation loops. In: Proceedings of International Conference on Advances in Mechanical & Automation Engineering, 7−8 June, Rome, Italy.

Nikuradse, J., 1950. Laws of Flow in Rough Pipes. NACA Technical Memorandum 1292, Washington, DC.

Pathirana, V., Chvala, O., Skutnik, S., 2021. Depletion dependency of molten salt reactor dynamics. Ann. Nucl. Energy 168, 1−15.

Pini, A., Cammi, A., Luzzi, L., Ruiz, D.E., 2014. Linear and nonlinear analysis of the dynamic behaviour of natural circulation with internally heated fluids. In: Proceedings of NUTHOS-10, Paper NUTHOS10−1074, 14−18 December 2014, Okinawa, Japan.

Pini, A., Cammi, A., Luzzi, L., 2016. Analytical and numerical investigation of the heat exchange effect on the dynamic behaviour of natural circulation with internally heated fluids. Chem. Eng. Sci. 145, 108−125.

Pope, S.B., 2000. Turbulent Flows. Cambridge University Press, UK.

Poppendiek, H.F., 1954. Forced-convection heat transfer in pipes with volume-heat sources within the fluids. Chem. Eng. Prog. Symp. Ser. 50 (11), 93−104.

Qiu, S., Zhang, D., Liu, L., Liu, M., Xu, R., Gong, C., et al., 2016. Coupled neutronics/thermal-hydraulics and safety characteristics of liquid-fueled Molten Salt Reactors. Kerntechnik 81, 149−159.

Ramzy, A., Bhaskar, M., Ziyad, S., Balestra, D., Fiorina, P., Hou, C., et al., 2020. Preliminary design and analysis of liquid fuel molten salt reactor using multi-physics code GeN-Foam. Nucl. Eng. Des. 369, 1−14.

Robertson, R.C., 1971. Conceptual design study of a single-fluid molten-salt breeder reactor. Technical Report, ORNL-4541.

Ruiz, D.E., Cammi, A., Luzzi, L., 2015. Dynamic stability of natural circulation loops for single phase fluids with internal heat generation. Chem. Eng. Sci. 126, 573−583.

Serp, J., Allibert, M., Benes, O., Delpech, S., Feynberg, O., Ghetta, V., 2014. The molten salt reactor (MSR) in generation IV: overview and perspectives. Prog. Nucl. Energy. 77, 308−319.

Sieder, E.N., Tate, G.E., 1936. Heat transfer and pressure drop of liquids in tubes. Ind. Eng. Chem. 28 (12), 1429−1435.

Tiberga, M., Gonzalez, R., Cervi, E., Blanco, J., Lorenzi, S., Aufiero, M., et al., 2020. Results from a multi-physics numerical benchmark for codes dedicated to molten salt fast reactors. Ann. Nucl. Energy 142, 1−19. 2020, 107428.

Todreas, N.E., Kazimi, M., 1990. Nuclear Systems, Thermal Hydraulic Fundamentals, Volume I. CRC Press, USA.

Vijayan, P.K., Sharma, A.K., Saha, D., 2007. Steady state and stability characteristics of single- phase natural circulation in a rectangular loop with different heater and cooler orientations. Exp. Ther. Fluid Sci. 31, 925−945.

Wan, C., Hu, T., Cao, L., 2020. Multi-physics numerical analysis of the fuel-addition transients in the liquid-fuel molten salt reactor. Ann. Nucl. Energy 144, 1−11. 107514.

Wilcox, D.C., 2006. Turbulence Modeling for CFD. DCW Industries, Inc., La Cañada, CA.

Yang, J., Oka, Y., Ishiwatari, Y., Liu, J., Yoo, J., 2007. Numerical investigation of heat transfer in upward flows of supercritical water in circular tubes and tight fuel rod bundles. Nucl. Eng. Des. 237 (4), 420–430.

Yu-ting, W., Bin, L., Chong-fang, M., Meng, Y., Hang, G., 2009. Convective heat transfer in the laminar-turbulent transition region with molten salt in a circular tube. Exp. Ther. Fluid Sci 33, 1128–1132.